Enhanced Sol-Gel Production and Robocasting for Artificial Photosynthesis

Frank Parsons and Ben Caroway

Abstract

In modern society, the demand for energy is becoming more immense year after year. While fossil fuels are inexpensive and easy to process, they have posed many safety issues and threats to the environment. For this reason, renewable technologies and the materials used in their development have become an important topic of research. Artificial photosynthesis, or the conversion of simple compounds (water, carbon dioxide) to burnable gases (hydrogen, methane), is a recently developed method that could produce clean, renewable fuel. In this study, improved fabrication and robocasting of Sol-Gel, a high viscosity fluid was explored. When solidified, Sol-Gel can catalyze reactions of liquid water and carbon dioxide gas to produce methane, a natural gas that can be used as fuel in power plants. The Sol-Gel process, which involves evaporating a precursor mixture to obtain a condensed solution, can take from 12 to 14 hours to complete. This method of fabrication is time consuming and difficult to control, so more efficient procedures were developed. In this study, a rotary evaporator was used to rapidly spin, heat, and remove solvents from Sol-Gel solution. This alternative system drastically reduced the time needed to produce condensed material–from 12 hours to ~10 minutes. In addition to improving the Sol-Gel process, 3D printing of the solution was investigated. Using a modified thermoplastic 3D printer, material was robocasted with an air pressure system. This device was able to print single line segments of Sol-Gel with reasonable quality, however it struggled to build structures exceeding more than one layer in height. While the robocaster was incapable of printing high surface area cells for artificial photosynthesis, this study proved the feasibility of a simplified 3D printer to extrude Sol-Gel.

Introduction

In 2017, the United States consumed approximately 97.7 quadrillion British thermal units

(btu) of energy (Energy Information Administration, 6, 2018). To put this figure into perspective, one btu is equivalent to the amount of energy released from burning a single match (Energy Information Administration, 7, 2018). From combustion in cars to household electricity, global power consumption has dramatically increased over the past decade. However in recent years, a slight decline in energy usage has also been observed. (Energy Information Administration 6, 2018). As modern innovation has improved the efficiency of power hungry devices such as light bulbs, computers, phones, and many other electrically operated machines, total electricity consumption has decreased. Despite these recent advancements however, as the global population continues to rise, and humans become increasingly reliant on technology to manufacture goods and store information, it will be crucial to research newer, more efficient methods of electricity generation.

According to the Energy Information Administration, 90% of the 97.7 quadrillion btu was generated through non-renewable fossil fuels (petroleum, coal, natural gas). This overwhelming preference for non-renewable technology can be attributed to several factors. Fossil fuels are inexpensive to obtain, exist in a relative abundance across the globe and they can be easily burned to produce vast amounts of energy. A major caveat when considering the use of fossil fuels, is their environmental impact in the forms of pollution and global warming (NASA, 2018). Renewable energy devices, which have little contribution to pollution or global warming, have been gaining in popularity in the last decade and are often a center of scientific research. Photovoltaics and wind turbines, which compose ~27% of renewable energy in U.S. energy reports, are of special importance when it comes to the discussion of clean energy because they are the only two methods of energy production which have almost no environmental impact. Biomass and hydroelectric energy systems are also renewable, but can pollute the environment.

The burning of biomass produces an extraordinary amount of greenhouse gas and hydroelectric dams have a significant effect on habitats of aquatic life (Energy Information Administration, 5, 2018). For these reasons, solar and wind energy seem like the most obvious choice for a renewable source, however, they also have some notable drawbacks. Solar energy suffers from a low electric conversion efficiency of around 15% even with peak environmental conditions and wind poses the expensive manufacturing costs of windmills (EURELECTRIC & VGB Powertech, 2003).

An important concept to consider when trying to improve the state of renewable energy technology is the global infrastructure of electric grids, which are heavily based upon fossil fuel power plants. In order to make a societal conversion to clean energy devices, a method of producing fossil fuels using renewable technology may be the best solution for avoiding expensive replacement of non-renewable systems. Natural gas, in particular, is a heavily used fossil fuel that could be derived through renewably powered chemical reactions, rather than through the fracking of gas deposits (Energy Information Administration, 8, 2018). One possible method of producing natural gas in a renewable fashion is through photochemical processes, which use light in combination with simple compounds such as water and carbon dioxide to produce clean burning gases like methane (Zhou et al, 2013).

When looking for a photochemical reaction to produce methane, the commonly known photosynthesis of plants comes to mind as a model for inspiration, due to its prevalence in nature and clever ability to alter simple compounds. Plants utilize carbon dioxide, water, and sunlight to produce glucose, a compound that can be stored and used to power biological processes (Farabee, 2007). However, one problem with glucose is that it serves little to no purpose for humans, as their scheme for producing energy revolves around the burning of gases and

flammable substances to produce electricity. For this reason, artificial photosynthesis, or the converting of simple molecules (water, carbon dioxide) into natural gases (hydrogen, methane) has been developed as an alternative to the reactions that produce glucose (Nocera, 2012). Using metal oxides (titanium, zinc, cobalt) as catalyst materials and a light source for power, water and carbon dioxide can be electrolyzed to form methane gas (Zhou et al, 2013). In order to make artificial photosynthetic reactions efficient, high surface structures and materials are needed for adequate gas output. For plants, the thylakoid, or sub-organelle structure that handles the primary reactions of photosynthesis is used to maximize energy production. When exposed to direct sunlight, thylakoid groupings will spread out to increase surface area and inversely, when eclipsed from sunlight, they will condense, uniting together to maximize efficiency under a low supply of power (Iwai et al, 2014). Using knowledge of both thylakoid structures and photosynthesis, various manufacturing techniques can be used to develop artificial photosynthetic cells (Zhou et al, 2013).

While the biomimicry inspired design of artificial photosynthesis provides a novel method of natural gas production, the processes used to manufacture photochemical devices are often complex and require expensive equipment. In order to improve both the speed and ease of renewable technology fabrication, 3D printing has been introduced as a solution to simplify the artificial photosynthetic process (Chen et al, 2018). While most 3D printers are based around the extrusion of thermoplastics such as polylactic acid (PLA), the principle of melting and layering a substance can be applied to a multitude of materials. In 2016, Harvard materials scientists 3D printed with custom designed inks that could interface with human cardiac tissue. This so called “heart-on-a-chip” technology was able to monitor heart conditions and even identify disease. Devices like these are an impressive display of 3D printing technology and highlight its diverse

range of applications (Burrows, 2016). To print photochemical devices that can catalyze the reaction of water and carbon dioxide to produce methane, a homogenous solution is needed for extrusion from a single nozzle (Duoss et al, 2007). One recently developed solution, known as Sol-Gel, is a high viscosity fluid that contains titanium based molecules which can be used for photochemical reactions. Sol-Gel starts out as a precursor solution, composed of several other chemicals. It then undergoes an evaporation process to produce a final condensed version that can be used for 3D printing into various structures (Cho et al, 2011). Once solidified, Sol-Gel is a rigid, ceramic-like material that can power surface reactions of liquid water and carbon dioxide gas to produce natural gases such as carbon monoxide and methane (Chen et al, 2018).

While Sol-Gel is an ingenious way to 3D print with functional materials, procedures to create the material are quite time consuming. Once Sol-Gel precursor has been mixed, the evaporation process to yield condensed solution can take anywhere from 12 to 14 hours (Duoss et al, 2007). Since the goal of Sol-Gel production is to quickly remove unwanted solvents, increased heating and agitation can drastically improve evaporation efficiency. This study was an attempt to decrease Sol-Gel reduction time with the use of a rotary evaporator. Through the repetitive movement of a rotating arm and a heated bath, the rotary evaporator provided an effective method of solvent reduction (Lab Society, n.d.). Sol-Gel is an important solution, crucial to the building of artificial photosynthetic cells and renewable technology. This experiment aimed to develop the materials science of Sol-Gel in order to reduce the complexity of its fabrication process and make it a more accessible to manufacturers.

Another objective in this study was to simplify the robocasting of Sol-Gel in a 3D printing system. Robocasting is the process of 3D printing with alternative materials such as ceramic, clay, or Sol-Gel (Euroceram, 2017). In studies such as Duoss et al. (2007), Cho et al.

(2011), and Chen et al. (2018), Sol-Gel was layered in an expensive robocasting 3D printer equipped with a glass microbore nozzle. Since machines like these take up large amounts of space and are complex to operate, a simplified system was devised. Utilizing an air compressor, pressure regulator, and pneumatic solenoid valve, movements of the 3D printer were synced with extrusion of the solution (Holzman and Francis, 2017). While printing of Sol-Gel in a simplified robocasting system only produced small structures, this study showed an easy method of 3D printing to fabricate functional materials.

Methods and Results

Investigations of Sol-Gel in this study were two fold: the first objective was to test the effect of rotary evaporation on Sol-Gel viscosity. This gave an indication of whether the material produced during rotary evaporation was of measurable quality to Sol-Gel produced with traditional methods (evaporation with a hot-plate). The second objective involved measuring Sol-Gel lines extruded from a robocasting 3D printer. The goal of this was to prove that a modified printer could produce Sol-Gel microstructures comparable to those of other studies: Duoss et al. (2008), Cho et al. (2011), and Chen et al. (2018).

Sol-Gel Mixing and Preparation (METHODS 1)

In order to derive condensed Sol-Gel solution, two different mixtures were prepared. The following chemicals were added to a 20 milliliter (mL) flask: titanium diisopropoxide acetylacetonate (TIA, 75 wt% dissolved in isopropanol, **8.33 mL**), polyvinylpyrrolidone (PVP, **0.33 g**), ethyl alcohol (ethanol, 99.5% pure concentration, **4 mL**). In a 100 mL beaker, additional chemicals were added: ethanol (**4 mL**), ammonium hydroxide solution (29% concentration, **0.67 mL**), and distilled water (**0.93 mL**). After both solutions were prepared, the beaker contents were

poured into the flask. Upon combining precursor materials, an IKA RV 10 rotary evaporator was used to reduce Sol-Gel for 3D printing. The 20 mL flask was attached to the evaporator rotating arm, which was angled into an IKA HB 10 heated bath filled with mineral oil (boiling point ~300°C). This allowed for heating and evaporation of ethanol, which has a boiling point of ~80°C. Water was also tested in the bath, however it quickly evaporated at 80°C and was not suitable for solvent reduction. During removal of ethanol in the evaporator, Sol-Gel volume went from roughly 20 mL to 5 mL in ~10 minutes. For this significant decrease, a vacuum pump rated at 15 pounds per square inch (psi) was used to draw ethanol vapors into the evaporator condensing coil–a glass tube filled with cold water. To supply the coil, two, gallon jugs were filled with ice water and attached to the evaporator via an aquarium pump. Solvents were then liquified by the coil and eventually discarded from an additional flask.

Sol-Gel preparation happened at various speeds and settings during this study. All samples were heated to 80°C and rotated at 120 revolutions per minute (rpm), however vacuum pressure was varied. About half of the samples were reduced at 500 millibars (mbar), which resulted in production times ranging from 10 to 20 minutes. The other half was exposed to 400 mbar with times from 5 to 10 minutes. Sol-Gel was removed from the evaporator once it began to bubble and darken in hue. This indicated a sufficient increase in viscosity for 3D printing.

Measuring the Dynamic Viscosity of Sol-Gel with a Ball-Drop Viscometer (RESULTS 1)

Dynamic viscosity, or the measure of a fluid's internal resistance to flow, was calculated by dropping steel balls through pipette tubes containing Sol-Gel. About 5 mL of both precursor and condensed material were added to 10 mL tubes and placed in front of a cell phone camera. 4.5 millimeter (mm) BBs were dropped down each tube and filmed for further analysis. Videos

were imported into *Vernier Logger Pro* software using a video analysis script and the movement of each ball was tracked frame by frame. In order to calculate the viscosity of a solution using a ball drop viscometer, various parameters about the ball and Sol-Gel were required: the ball's density and diameter as well as the fluid's density. Using the time it takes for the ball to descend through the solution at terminal (constant) velocity and the length of the drop, viscosity was calculated using an equation developed by Tang et al. (2016). Utilizing Stokes' Law: $f = 6\pi\eta r v$, where f equals the viscous drag force exerted on the ball,η, or the fluids viscosity can be solved for by deriving a terminal speed of the ball.

$$v_f = \frac{2r^2(\rho_b - \rho_f)g}{9\eta}$$

η = Fluid Viscosity g = Gravitational Acceleration
r = Ball Radius v_f = Terminal Velocity
ρ_b = Ball Density
ρ_f = Fluid Density

The final viscosity was then evaluated through this equation:

$$\eta = \frac{d^2(\rho_b - \rho_f)gT}{18L}$$

η = Fluid Viscosity g = Gravitational Acceleration
d = Ball Diameter T = Time to Fall *L* Distance
ρ_b = Ball Density L = Length of Drop
ρ_f = Fluid Density

Three BB drops (trials) were filmed and analyzed for both the precursor and condensed Sol-Gels. An example of viscosity calculation is shown in figure 1.

Figure 1. *Apparent Viscosity of Precursor Sol-Gel Trial 1*

$$\frac{(4.5)^2\,(7.22 - 1.195)\,(9.806)\,(5.7667 - 4.7667)}{18\,(32.8823 - 7.6760)}$$

$$= 2.6368 \text{ centipoise (cP)}$$

This calculation was repeated six times: three for the precursor Sol-Gel trials and three for the condensed Sol-Gel trials. The values used for each equation are displayed in tables 1-4.

Table 1. *Material Measurements*

Measured Item	Measurement
Diameter of ball (d)	4.5 mm
Mass of ball (m_b)	0.3442 g
Mass of Precursor Sol Gel (m_p)	1.1950 g
Volume of Precursor Sol Gel (v_p)	1.000 mL
Mass of Condensed Sol Gel (m_p)	0.9900 g
Volume of Condensed Sol Gel (v_p)	1.000 mL

Table 2. *Material Calculations*

Measured Item	Formula	Calculated Value
Radius of ball (r)	$r = d/2$	2.3 mm = 0.23 cm
Volume of ball (v)	$v = 4/3\pi r^3$	0.0477 mL
Density of ball (ρ_b)	$\rho_b = m_b / v_b$	7.22 g/mL
Density of Precursor Sol Gel (ρ_p)	$\rho_p = m_p / v_p$	1.195 g/mL
Density of Condensed Sol Gel (ρ_c)	$\rho_c = m_c / v_c$	0.9900 g/mL

Table 3. *Video Analysis Time (T) Measurements*

Substance	Trial Number	Total Time (s)
Precursor Sol Gel	1	1.000
Precursor Sol Gel	2	1.000
Precursor Sol Gel	3	0.966
Condensed Sol Gel	1	67.598
Condensed Sol Gel	2	112.763
Condensed Sol Gel	3	115.766

Table 4. *Video Analysis Distance (L) Measurements*

Substance	Trial Number	Total Distance (cm)
Precursor Sol Gel	1	25.206
Precursor Sol Gel	2	25.162
Precursor Sol Gel	3	25.606
Condensed Sol Gel	1	10.360
Condensed Sol Gel	2	11.986
Condensed Sol Gel	3	10.873

After viscosity was calculated with the equation and values shown above, additional formulas were required to convert this *apparent viscosity* measured through the cell phone camera to *absolute viscosity*, adjusted against water.

$$\frac{\text{Apparent Viscosity of Water}}{\text{Absolute Viscosity of Water}} = \frac{\text{Apparent Viscosity of Test Substance}}{\text{Absolute Viscosity of Test Substance}}$$

A sample of water was also tested in the viscometer to compare with its absolute viscosity of 1.002 cP. The values shown in tables 5 and 6 were used to calculate the apparent viscosity of water in the ball-drop viscometer.

Table 5. *Video Analysis Time (T) Measurements for Water*

Substance	Trial Number	Total Time (s)
Water	1	0.933
Water	2	1.169
Water	3	0.933

Table 6. *Video Analysis Distance (L) Measurements for Water*

Substance	Trial Number	Total Distance (cm)
Water	1	30.904
Water	2	31.850
Water	3	31.827

The final calculations for both apparent and absolute viscosities are expressed in table 7.

Table 7. *Viscosity Calculations*

Material	Trial	Apparent Viscosity Calculation based on Ball Drop Experiment (cP)	Viscosity (cP) adjusted against water
Water	1	2.072	N/A
	2	2.519	N/A
	3	2.012	N/A
	Avg.	2.201	N/A
Precursor Sol-Gel	1	2.636	1.200
	2	2.641	1.202
	3	2.509	1.142
	Avg.	2.595	**1.181**

Condensed Sol-Gel	1	448.41	204.12
	2	646.58	294.34
	3	731.74	333.10
	Avg.	608.91	**277.19**

The final estimate of viscosity for rotary evaporator Sol-Gel ranged between 1.14 and 1.2 cP for the precursor and from 204 to 277 cP for the condensed. To verify this approach of data collection, measurements from Duoss et al. (2007) were used for comparison. The final values are expressed expressed in figures 2 and 3.

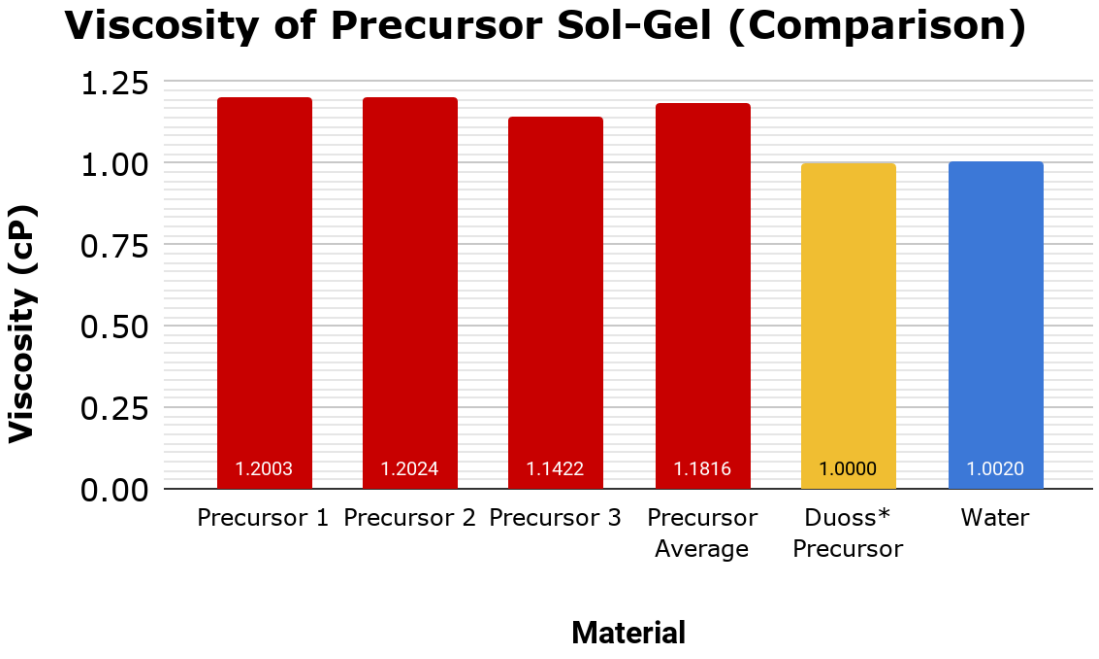

Figure 2. Displays the absolute viscosity of precursor Sol-Gel in trials 1, 2, 3, and their average. Also shows the viscosity of water at 20°C.

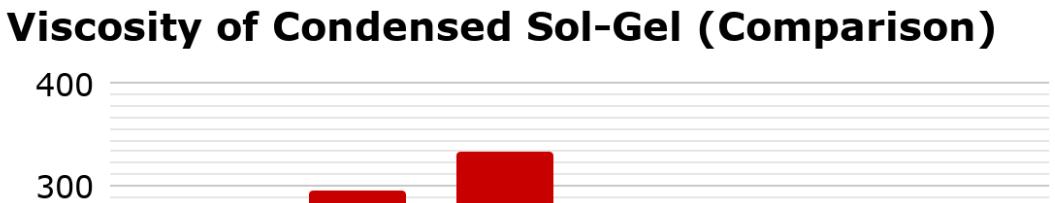

Figure 3. Displays the absolute viscosity of condensed Sol-Gel in trials 1, 2, 3, and their average. Also shows the viscosity of water at 20°C and the viscosity of condensed Sol-Gel fabricated by Duoss et al. in 2007

Robocasting with a Desktop 3D Printer (METHODS 2)

After the creation of condensed solution, a 3D printer was used to fabricate Sol-Gel structures. Most desktop 3D printers–like the one used in this study–print with thermoplastics such as PLA. Since this method is not suitable for printing with high viscosity fluids, a robocasting system was installed to extrude Sol-Gel. First, the original thermoplastic hot end was removed from the print head and replaced with a syringe. Sol-Gel was poured into the syringe and pushed by a stopper, which was connected to an air pressure system composed of the following components: a pneumatic solenoid valve, pressure regulator and an air compressor rated from 0 to 115 psi.

Pneumatic solenoid valves have a coil that oscillates back and forth based the output of an electromagnet. When the electromagnet is active, a small metal rod slides forward and stops the flow of air. This was used to coordinate 3D printer movements with the extrusion of Sol-Gel. The rest of the system fit to together in the following sequence: vinyl tubing rated for 140 psi was passed from the compressor, through the digital pressure regulator, solenoid valve, and to the syringe. The solenoid valve was also powered and connected to the printers microcontroller, which is a programmable circuit used to control motors of the 3D printer. After assembly of robocasting components, a 3D model was needed to operate the 3D printer. The computer-aided design (CAD) program *Autodesk Maya* was used to generate simple rectangular shapes for Sol-Gel extrusion. A rendering of these models is shown in the figure below.

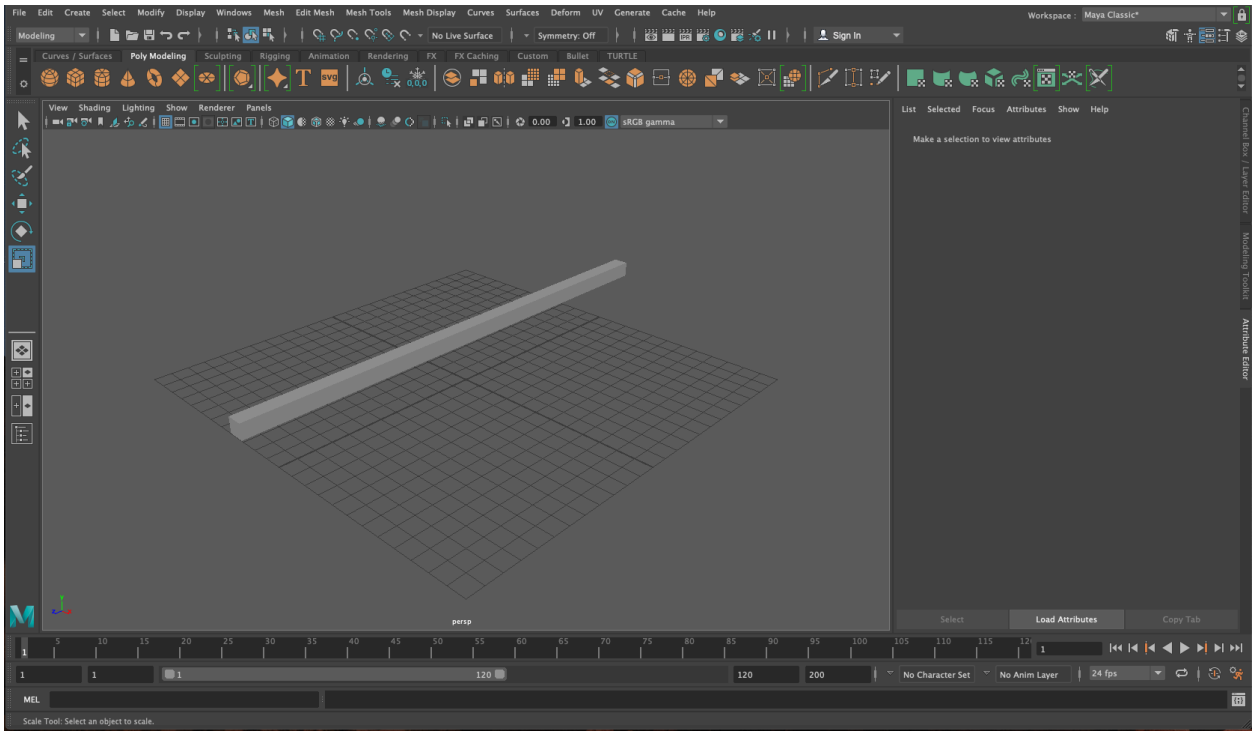

Figure 4. Displays Autodesk Maya build window with a rectangular prism.

To translate these models into executable code for the 3D printer, a program called *Slic3r* was used. With printer dimensions and hardware as reference, Slic3r split the rectangular object into several layers, which were used to build the 3D model over a series of printer movements. Code generated from Slic3r was formatted in a file type known as *Gcode*, which is a special machine programming language for 3D printers. Gcode consists of single line commands, each with a letter followed by a number. Examples of Gcode can be found in figure 5.

LineTest.gcode

```
; generated by Slic3r 1.2.9 on 2018-12-17 at 22:22:23

; external perimeters extrusion width = 0.53mm
; perimeters extrusion width = 0.56mm
; infill extrusion width = 0.56mm
; solid infill extrusion width = 0.56mm
; top infill extrusion width = 0.56mm

M104 S200 ; set temperature
G28 ; home all axes
```

Figure 5. Displays Gcode generated from the "Sol-Gel Line Test" (described in proceeding section)

Before the Gcode was loaded onto the printer's SD card, edits were made to control the solenoid valve. By replacing the unretract and retract commands listed above with "M106 S0" and "M106 S255," the solenoid valve was toggled on and off through the use of a digital pin on the printer's microcontroller. This allowed for Sol-Gel extrusion to only be active during fabrication of each 3D model. These Gcode edits are displayed in the figure below.

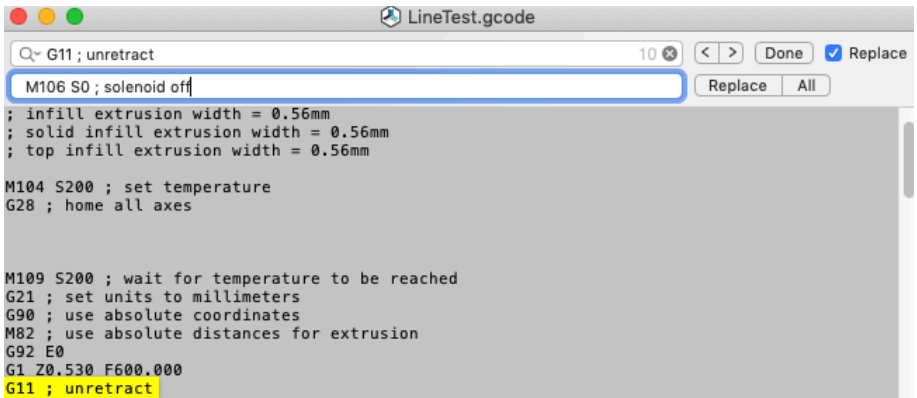

Figure 6. Shows the use of find & replace to change all retraction commands to solenoid valve commands.

Before

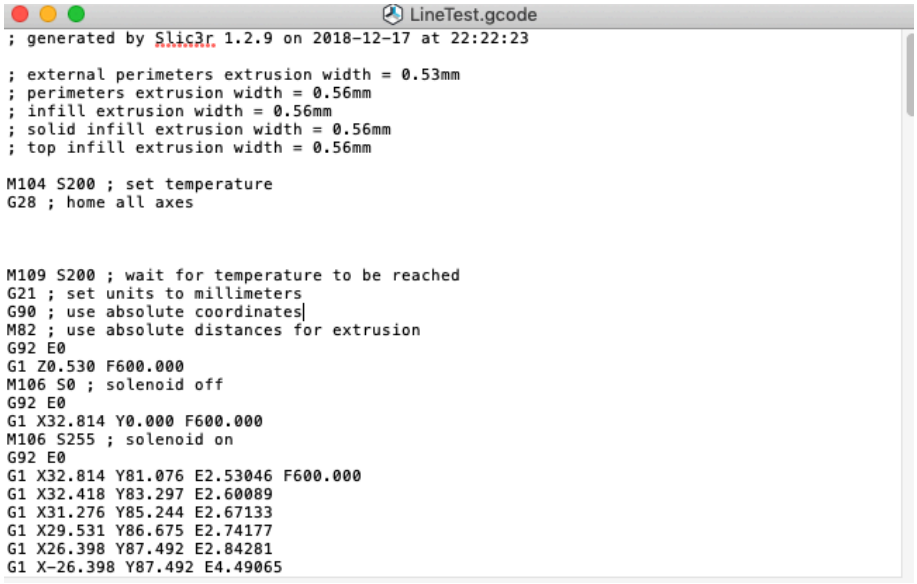

After

Upon modifying the Gcode, it was copied onto an SD card and inserted in the printer's microcontroller.

Testing the Robocasting System with a Sol-Gel Line Test (RESULTS 2)

After the creation of a robocasting system and rectangular 3D model, a line test was prepared for the 3D printer. This involved the printing of several Sol-Gel line segments. To start, small acetate plastic circles were taped to the print bed for later removal and observation. The air compressor was pumped up to about 20 psi and the Sol-Gel was loaded into a syringe. To test

flow properties from the print head, five different needle sizes were used: 160, 260, 340, 410, 510 micrometers (um).

Figure 7. Shows the color and size of each needle.

The first needle was attached, then the print was started. After one line, the code was stopped and a new needle was applied. This process was repeated for each needle size. For each sample, the plastic circle was removed from the printer and placed under an optical microscope for analysis. At ~7.5x zoom, a ruler with millimeter markings was placed on top of the line segments. Pictures of the enlarged Sol-Gel were taken using a camcorder and television attached to the microscope. These images were then imported into *ImageJ* and measured using built-in scale tools. To do this, the millimeter markings were recorded in the program as a certain number of pixels on the image and used calculate Sol-Gel line widths. All of the samples were measured in 20 different places to derive an average width for each needle size. These results are in the figure below.

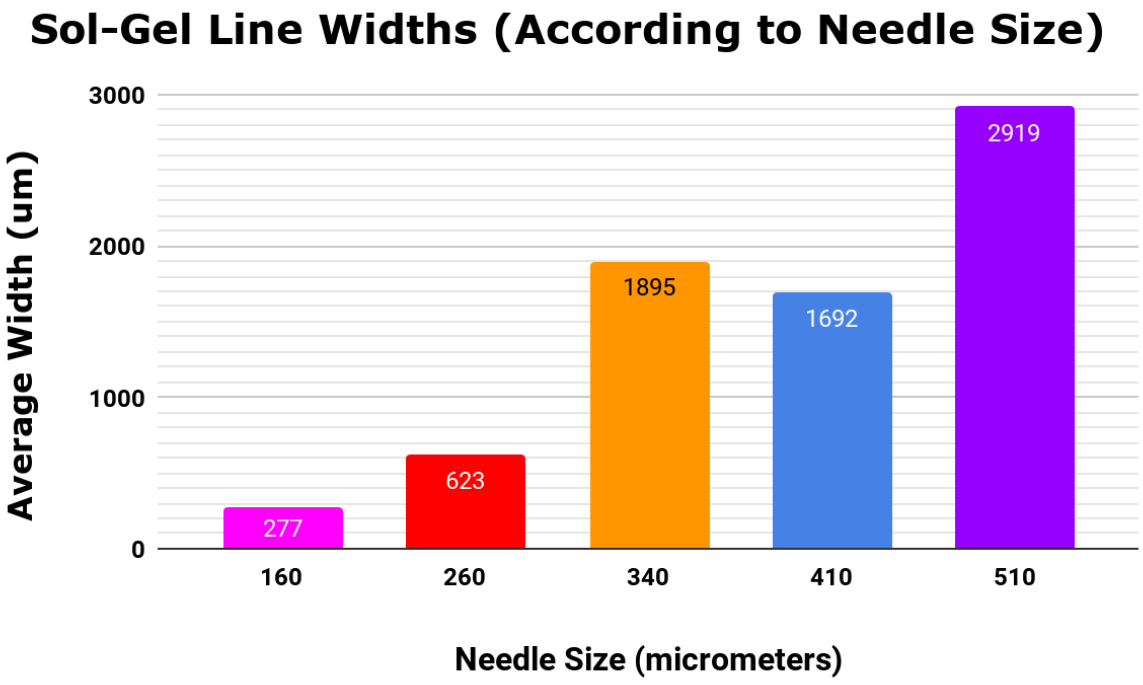

Figure 8. Displays the average width of Sol-Gel line for each needle size in micrometers.

After all sizes were calculated, line width was divided by needle size for each value. The purpose of this was determine whether a change in needle size resulted in a comparable effect on width. Those calculations are in the figure below.

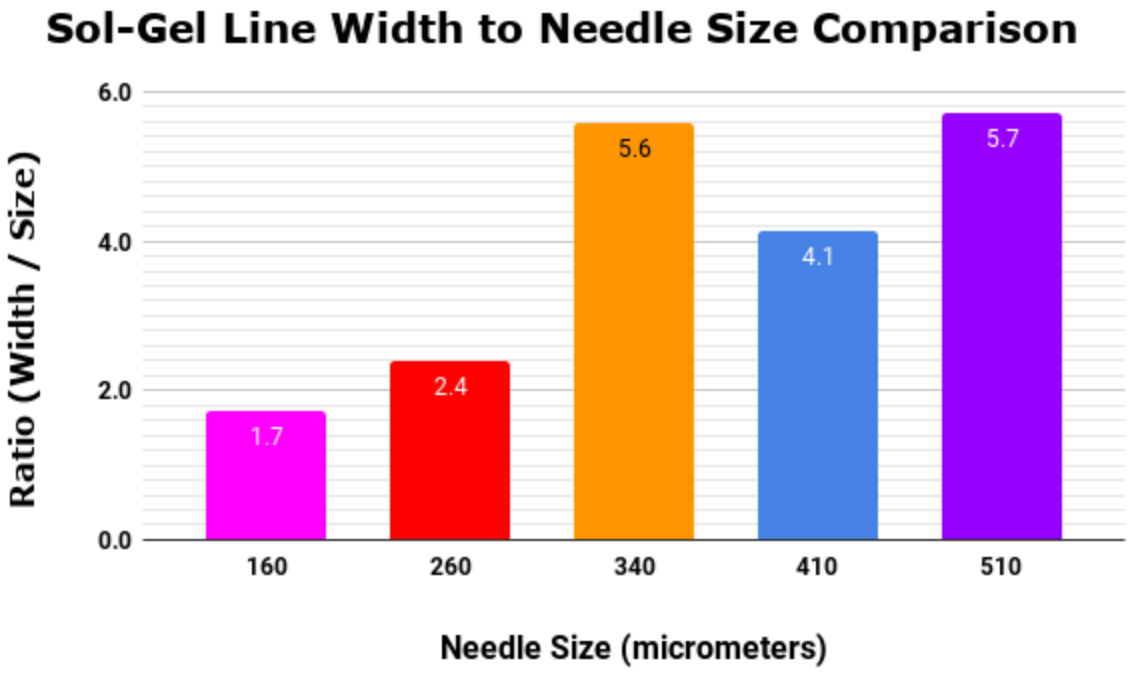

Figure 9. Displays the ratio of line width to needle size.

Discussion

Dynamic Viscosity of Sol-Gel with a Ball-Drop Viscometer

Viscosity tests in this study produced remarkable results. By using a simple pipette tube and steel ball, dynamic viscosity of Sol-Gel was estimated with reasonable accuracy. In Tang et al. (2016), viscosity of 50% glycerol solution was calculated using a similar ball-drop viscometer. Their device produced a value of 4.43 centipoise, which compared to their reading of 4.68 cP from a more sophisticated *Cannon-Fenske viscometer* is quite exceptional. These comparisons helped to verify the ball-drop approach of finding Sol-Gel viscosity. However, one caveat to this procedure was any human error present in viscometer construction, ball filming or video analysis. In Tang's paper, he suggests a 5 to 10% error in viscosity values dependent upon how meticulous measurements are taken. Since he used a simple stopwatch setup, manually

timing each drop, the Vernier video analysis of this study may have improved the measurement process. The estimates of 204 and 330 cP for condensed Sol-Gel also came strikingly close to Duoss et al. measurements of 210-420 cP. This further affirmed the validity of ball-drop viscosity procedures. In order to derive an a more representative average of condensed Sol-Gel viscosity, future tests should involve multiple ball drops and different consistencies of Sol-Gel to rule out any error in experimental design.

Sol-Gel Line Test

Extrusion of Sol-Gel in the robocasting 3D printer was observed through an optical microscope. With the help of a ruler, measurements were made at an accuracy of 1 millimeter (mm). The millimeter was considered a significant figure because there was no way to precisely distinguish smaller distances. An attempt was made to estimate micrometer sized widths using image analysis software, however camera distortion and the microscope's weak resolving power lead to questionable image quality. In order to clarify the detail of Sol-Gel microstructures, a scanning electron microscope (SEM) or more advanced tool is required. Despite these issues with analysis, reasonable width comparisons were made between needle sizes. Sol-Gel line widths ranged from roughly a third of a millimeter to 3 mm. It was observed that as needle size increased, segment width increased rapidly, if not exponentially. Since the solid particles in Sol-Gel are large in diameter, there is a narrow threshold at which material flow begins to drastically flow. This is one possible explanation for the behavior exhibited in these results. Most the line test data made sense with regard to needle size, however one discrepancy between the 360 and 410 um segments was noted. Irregularity in extrusion pressure is most likely the cause as the pressure regulator could only maintain within 2 to 3 psi of the target pressure (20 psi). Other possible complications include contamination in the needle, leaking in the air supply tube,

or inconsistency in the Sol-Gel itself.

Conclusion

This study showed an effective use of rotary evaporator technology to improve the production of Sol-Gel. In traditional fabrication of robocasting fluids, a significant amount of reduction time is needed to remove solvents. In several reports of Sol-Gel production such as Duoss et al. (2008), Cho et al. (2011), and Chen et al. (2018), they utilized a simple hot-plate setup to evaporate and condense each sample, taking upwards of 10 to 14 hours to completely remove unwanted fluids. Through the use of a vacuum pump and rotating arm, Sol-Gel in this experiment was quickly processed, with reduction times ranging from 7 to 20 minutes. In addition to a significant time compression, the material produced through these methods had viscosities ranging from 204 to 330 centipoise. According to Duoss et al, optimal Sol-Gel viscosities for 3D printing are between 210 and 400 centipoise. With such a similar consistency, it was concluded that a rotary evaporator can dramatically streamline the production of Sol-Gel while still maintaining its printable qualities. In the papers by Duoss et al. (2008), Cho et al. (2011), and Chen et al. (2018), Sol-Gel was 3D printed through microbore needles with tips ranging from 1 to 100 micrometers in diameter. For the material to fully solidify and adhere to the print bed, these extrusion sizes were found to be the most optimal for printing complex structures. Due to air pressure system limitations, this study printed with larger needles sizes between 160 and 510 micrometers at 20 psi. It was found that the high content of solid materials in Sol-Gel causes extruded lines to grow exponentially in width as needle size increases. Since the printing of microscale line widths was unattainable, the modified robocasting system proved ineffective at fabricating any large or complex structures. However, in the future, simpler 3D printing systems could be used for construction of smaller components that are then assembled

into larger devices, capable of artificial photosynthesis.

Future Work

To improve the process of Sol-Gel production in a rotary evaporator, numerous variations on vacuum pressure and rotational speed should be tested to fully develop methods for consistent material fabrication. Varying the amount of solids in the solution should also be investigated for its effect on behavior in the rotary evaporator system. As for the robocasting 3D printer, quality of Sol-Gel extrusion should be improved through alteration of the air pressure system. For instance, a printer equipped with a liquid powered extruder may be more suitable. Air, while easy to work with, is hard to control because of its ability to quickly expand and contract. One possible solution to this problem is the use of water, oil, or another liquid in a hydraulic control device. Through the use of a positive displacement pump or other type of valve, fine tuned extrusion of Sol-Gel could be achieved.

After Sol-Gel has been printed and solidified, its main function is to catalyze the reaction between carbon dioxide and water to produce methane. While this studied primarily focused on the structural and behavioral properties of the material, further research into the chemically active components of rotary evaporator Sol-Gel is needed. In earlier work, a testing chamber was constructed as a possible method to contain and monitor the output of methane from dried Sol-Gel. The Artificial Photosynthetic Testing Chamber (APTC) was based around 4 MQ sensors positioned in a 1 gallon plastic fish tank. With two dedicated to the sensing of CO_2 consumption and two for CH_4 output, an Arduino microcontroller was connected to these devices to log data on an SD card. In an actual reaction of Sol-Gel, dry ice would be the carbon dioxide source, distilled water would be the other reactant and a 5000 lumen grow lamp would be the power source. Once more complex structures have been fabricated with the simple robocasting

system, an APTC could be used to describe the methane conversion efficiency of rotary evaporator Sol-Gel. In future work, biomimicry inspired designs such as a 3D modelled chloroplast or thylakoid membrane, would be worth exploring as way to produce high surface area devices that improve the reaction between carbon dioxide and water.

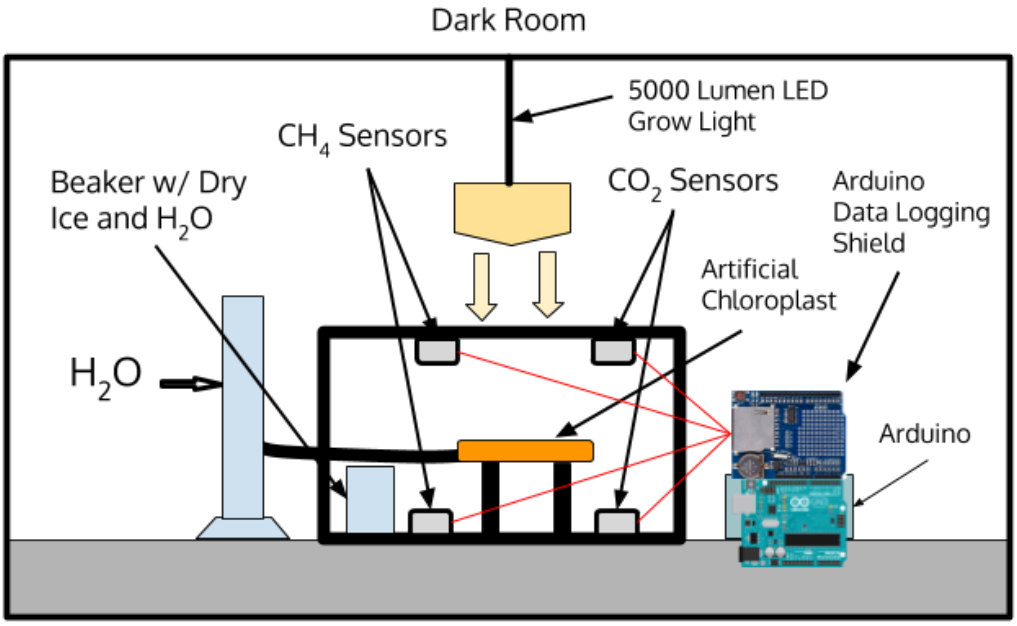

Figure 10. Diagram of the Artificial Photosynthetic Testing Chamber (APTC).

References

1. Burrows, L. (2016, October 25). Harvard Engineers Create the First Fully 3D-Printed Heart-on-a-Chip. Retrieved from https://scitechdaily.com/harvard-engineers-create-the-first-fully-3d-printed-heart-on-a-chip/

2. Chen, L., Tang, X., Xie, P., Xu, J., Chen, Z., Cai, Z., … He, P. (2018). 3D Printing of Artificial Leaf with Tunable Hierarchical Porosity for CO2 Photoreduction. *Chemistry of Materials*. https://doi.org/10.1021/acs.chemmater.7b04313
3. Cho, Y., Son, S., Kim, Y., Chung, K., & Choi, C. (2011). Development of Direct Ink Writing Technology for Micro-Structures. *Reviews on Advanced Materials Science*, *28*(2), 175-180. Retrieved from http://www.ipme.ru/e-journals/RAMS/no_22811/39_paper.pdf
4. Duoss, E., Twardowski, M., & Lewis, J. (2007). Sol-Gel Inks for Direct-Write Assembly of Functional Oxides. *Advanced Materials*, *19*(21), 3485-3489. https://doi.org/10.1002/adma.200701372
5. Energy Information Administration. (2018, July 13). Renewable Energy Sources - Energy Explained, Your Guide To Understanding Energy. Retrieved from https://www.eia.gov/energyexplained/index.php?page=renewable_home
6. Energy Information Administration. (2018, May 16). U.S. Energy Facts - Energy Explained, Your Guide To Understanding Energy. Retrieved from https://www.eia.gov/energyexplained/?page=us_energy_home
7. Energy Information Administration. (2018, August 8). Units and Calculator - British Thermal Units (Btu) - Energy Explained, Your Guide To Understanding Energy. Retrieved from https://www.eia.gov/energyexplained/index.php?page=about_btu

8. Energy Information Administration. (2019, January 16). Production of Hydrogen - Energy Explained, Your Guide To Understanding Energy. Retrieved from https://www.eia.gov/energyexplained/index.php?page=hydrogen_production
9. EURELECTRIC, & VGB Powertech. (2003). Efficiency in Electricity Generation. Retrieved from https://wecanfigurethisout.org/ENERGY/Web_notes/Bigger%20Picture/Where%20do%20we%20go%20-%20Supporting%20-%20Files/Efficiency%20in%20Electricity%20Generation%20-%20EURELECTRIC.pdf
10. Euroceram. (2017, December 13). Robocasting - Direct Ink Writing. Retrieved from http://www.euroceram.org/en/technologies/material-extrusion/robocasting-direct-ink-writing.html
11. Farabee, M. J. (2007). PHOTOSYNTHESIS. Retrieved from https://www2.estrellamountain.edu/faculty/farabee/BIOBK/BioBookPS.html
12. Holzman, N., & Francis, L. (2017). Pneumatic System Design for Direct Write 3D Printing. *Solid Freeform Fabrication Symposium*. Retrieved from http://sffsymposium.engr.utexas.edu/sites/default/files/2017/Manuscripts/PneumaticSystemDesignforDirectWrite3DPrinti.pdf
13. Iwai, M., Yokono, M., & Nakano, A. (2014). Visualizing structural dynamics of thylakoid membranes. *Scientific Reports*, *4*(1). http://doi.org/10.1038/srep03768
14. Lab Society. (n.d.). Rotary Evaporators & Solvent Recovery Products. Retrieved from https://labsociety.com/lab-equipment-category/rotary-evaporators/

15. Lloyd, D. (2014, December 11). Wind Energy: Advantages and Disadvantages. Retrieved from http://large.stanford.edu/courses/2014/ph240/lloyd2/

16. NASA. (2018, December 13). Climate change causes: A blanket around the Earth. Retrieved from https://climate.nasa.gov/causes/

17. Nocera, D. G. (2012). The Artificial Leaf. *Accounts of Chemical Research*, *45*(5), 767-776. http://doi.org/10.1021/ar2003013

18. Zhou, H., Guo, J., Li, P., Fan, T., Zhang, D., & Ye, J. (2013). Leaf-architectured 3D Hierarchical Artificial Photosynthetic System of Perovskite Titanates Towards CO2 Photoreduction Into Hydrocarbon Fuels. *Scientific Reports*, *3*(1). http://doi.org/10.1038/srep01667